Contents lists available at ScienceDirect

Surface & Coatings Technology

journal homepage: www.elsevier.com/locate/surfcoat

Inert gas effects on the deposition rate of TiO_2 during reactive HiPIMS

CrossMark

Michael Bowes, James W. Bradley *

Department of Electrical Engineering and Electronics, University of Liverpool, Brownlow Hill, Liverpool L69 3GJ, UK

ARTICLE INFO

ABSTRACT

Deposition rates have been measured during the reactive HiPIMS of Ti in the presence of oxygen and different inert gases (i.e. mixtures of X/O_2 where X = Ne, Ar, Kr or Xe) by means of a quartz crystal microbalance (QCM). The QCM was positioned above the erosion racetrack directly facing the target surface at two different axial distances (50 and 100 mm). The HiPIMS discharge was operated with a pulse on-time $\tau = 100$ μs, a pulse frequency $f = 100$ Hz and a constant average discharge power $P_{avg} = 100$ W (50 W for Xe/O_2). The oxygen partial pressure, p_{O2}, was maintained at a constant $0.2p_t$ where p_t is the total pressure and was maintained at a constant 0.4 Pa. Using these conditions, the discharge was operated in the so-called 'poisoned' mode. In contrast to the trends predicted by SRIM as well as those measured in DCMS, the power-normalized static deposition rates in reactive HiPIMS of titanium measured in gas mixtures of oxygen were observed to increase with the mass of the inert gas. The observed trend was attributed to a decreased *return effect* as a result of an increased average absolute target potential during the pulse on-phase when employing heavier inert gases as the buffer gas. For the case of Kr/O_2, the normalized deposition rate measured in HiPIMS was found to be 87% of that measured in equivalent DCMS operation.

© 2014 Elsevier B.V. All rights reserved.

1. Introduction

The main drawback of a newly emerging physical vapour deposition technology, high power impulse magnetron sputtering (HiPIMS) [1], is the almost universally reported reduced *power normalized* deposition rate when compared with conventional direct current magnetron sputtering (DCMS). The normalized deposition rate for non-reactive HiPIMS has been observed to be typically 30–85% [2,3] of the value measured during equivalent DCMS operation. There are several mechanisms thought to be responsible for this apparent reduction in deposition rate and they have been the subject of some recent publications [4,5]. Due to the increased ionization of sputtered species that occurs in a HiPIMS discharge there exists a so-called *return effect* whereby a non-negligible fraction of the ionized sputtered material is back-attracted to the target surface [4–6]. Another major issue is the less than proportional scaling of the sputter yield with incident ion energy, often referred to as the *yield effect* [4,7]. HiPIMS typically employs higher absolute target potentials when compared with DCMS and hence lower average ion currents are necessary for the same time-averaged power. The deposition rate is typically proportional to the sputter yield; however the sub-proportional scaling of sputter yield with incident ion energy results in a decreased normalized deposition rate for increased absolute target potential values. Other effects include the ion species effect [4], transport effects [8,9], coating effects [3,4], power-switching effects [4] and magnetic field effects [5]. Anders [4] has presented a detailed treatment of the main mechanisms affecting the deposition rate during non-reactive

HiPIMS. Also, Vlcek and Burcalova developed expressions for deposition rates in a phenomenological model for HiPIMS [10].

In reactive HiPIMS, the composition of the discharge and the extent of the target coverage/poisoning are important aspects to consider. In the case of sputtering oxides, the oxygen reacts with the target surface to varying degrees mostly dependent upon the ion contribution to the discharge current and the reactive gas flow rate resulting in a metallic target partially or completely covered ('poisoned') with a compound layer. It is known that many oxide compounds suffer from a lower deposition rate than their pure metal counterparts [11] and so the reduced normalized deposition rate in HiPIMS when compared with DCMS can be of great concern in reactive sputtering.

Furthermore, large amounts of high energy negative ions are generated during reactive DCMS [12–16] and reactive HiPIMS [17] in the presence of electronegative gases such as oxygen. It is possible that the bombardment of the substrate by the high-energy population of the negative ions will lead to resputtering of the growing film and result in a reduction of the effective deposition rate. Despite this, there are some promising aspects of reactive HiPIMS including hysteresis-free operation [18] and even deposition rates measured to be higher than those achieved in the equivalent DCMS process [18–20]. For example, Sarakinos et al. [18] found that the deposition rate of TiO_x thin films increased by up to 40% for HiPIMS of a $TiO_{1.8}$ target when compared with DCMS. Also, the measured deposition rates during the assisted HiPIMS of titanium have been correlated to the crystal formation phase of the deposited TiO_2 [21], meaning the deposition rate could be potentially used as a control parameter.

The work presented in this contribution focuses on the measured static normalized deposition rates of titanium oxide during reactive

---

* Corresponding author. Tel.: +44 151 794 4545.
  E-mail address: j.w.bradley@liverpool.ac.uk (J.W. Bradley).

HiPIMS of titanium in a gas mixture of X/O_2, where X = Ne, Ar, Kr or Xe. The primary mechanisms affecting the deposition rate are briefly discussed and deposition rates measured in reactive HiPIMS are compared to measurements made in nominally equivalent reactive DCMS discharges for $d = 100$ mm.

2. Experimental set-up

2.1. Arrangement of HiPIMS set-up

A cylindrical vacuum vessel with a length of 300 mm and a diameter of 260 mm equipped with a commercial circular planar unbalanced magnetron source (GENCOA Ltd.) was pumped down to a base pressure of approximately 5×10^{-4} Pa using a turbomolecular pump backed by a rotary pump. The magnetron was equipped with a new titanium target (99.95% purity) with a diameter of 75 mm and powered by a HiPIMS power supply built in-house, described in detail in [22].

In addition to the HiPIMS power supply, a low power (≤ 10 W) pre-ionization unit was used to facilitate operation at low pressure and to allow for greater reproducibility of pulse waveforms, which is also described in [22]. The switching of the HiPIMS power supply was triggered by an external pulse generator (Thandar TG105) by which the voltage pulse width τ and frequency f were controlled. In this investigation, the voltage pulse on-time and frequency were maintained constant at $\tau = 100$ μs and $f = 100$ Hz respectively.

Process gases were introduced into the chamber at flow rates controlled by two independent mass flow controllers (MKS 1179A). The total working gas pressure, $p_t = p_X + p_{O2} = 0.4$ Pa (X = Ne, Ar, Kr, Xe), was monitored using a capacitance pressure gauge (MKS 628A). All working gases used in this investigation were of a purity of at least 99.995%. A schematic of the experimental apparatus is given in Fig. 1.

To obtain the desired oxygen partial pressure, the oxygen flow rate was increased beyond the hysteresis transition from metallic to poisoned mode and then reduced as necessary to maintain a constant oxygen partial pressure; $p_{O2} = 0.2p_t$. The target voltage $V_d(t)$ was measured using a high voltage probe (Tektronix P5100) and the discharge current $I_d(t)$ was measured using a DC coupled current probe (Tektronix TCP202) which were both connected to a digital oscilloscope (Tektronix TDS3014, 100 MHz bandwidth). The average discharge power, P_{avg}, was monitored in real-time using the same oscilloscope, calculated as the mean of the product of $V_d(t)$ and $I_d(t)$ and controlled by manually varying the initial target potential V_0 provided by the power supply.

2.2. Deposition rate measurements

Deposition rates, were measured by means of a quartz crystal microbalance (QCM) with the exposed face of the gold-coated sensor crystal (6 MHz) grounded and the opposite side connected to a thin film deposition monitor (Maxtek TM-400, Inficon). The sensor crystal was placed directly above the racetrack facing the target surface at two different axial distances, $d = 50$ and 100 mm. Reading directly from the DAC output of the deposition rate monitor, the film thickness was monitored as a function of time using a voltage probe (Tektronix P6139A) over a period of 500 s. The output range of the monitor was 0 to 5 V, corresponding to a thickness range of 0 to 100 Å (i.e. a step of 0.05 V/Å). For calculation of the film thickness, the deposited film was assumed to be stoichiometric titania with a density of 4.26 g/cm². Prior to any deposition rate measurements, the discharge was operated in metallic mode with a pressure of 0.93 Pa in the presence of the relevant inert gas (zero oxygen flow) for 15 min in order to sputter-clean the target surface. Following the introduction of oxygen to the desired partial pressure, the discharge was operated for a further 15 min to obtain an equilibrium state. During this run-in procedure, the QCM was protected by a stainless steel shield, which could be removed without breaking vacuum. The same initial procedure was employed for each deposition rate measurement.

3. Results and discussion

3.1. HiPIMS pulse waveforms

Waveforms of the target discharge current $I_d(t)$ and potential $V_d(t)$ for the different gas mixtures (X/O_2 where X = Ne, Ar, Kr or Xe) are shown in Fig. 2. The discharge parameters were as follows: $P_{avg} = 100$ W, $f = 100$ Hz, $\tau = 100$ μs, $p_t = 0.4$ Pa and $p_{O2} = 0.2p_t$. For the case of Xe/O_2, the average discharge power was maintained at 50 W due to the power supply being unable to maintain an average discharge power of 100 W without lengthening the pulse on-time τ or increasing the pulse frequency f. For an increased mass of the sputtering ion, the Bohm velocity naturally decreases thereby increasing the transit time across the cathode sheath. In addition, and as discussed below, the reduction in the secondary electron emission coefficient for heavier inert gases explains the observed increase in the time taken for $I_d(t)$ to reach a maximum for increasing inert gas mass mixed with oxygen.

Also evident from Fig. 2 is a clear increase in required absolute target potential for heavier gas mixtures to maintain a constant discharge
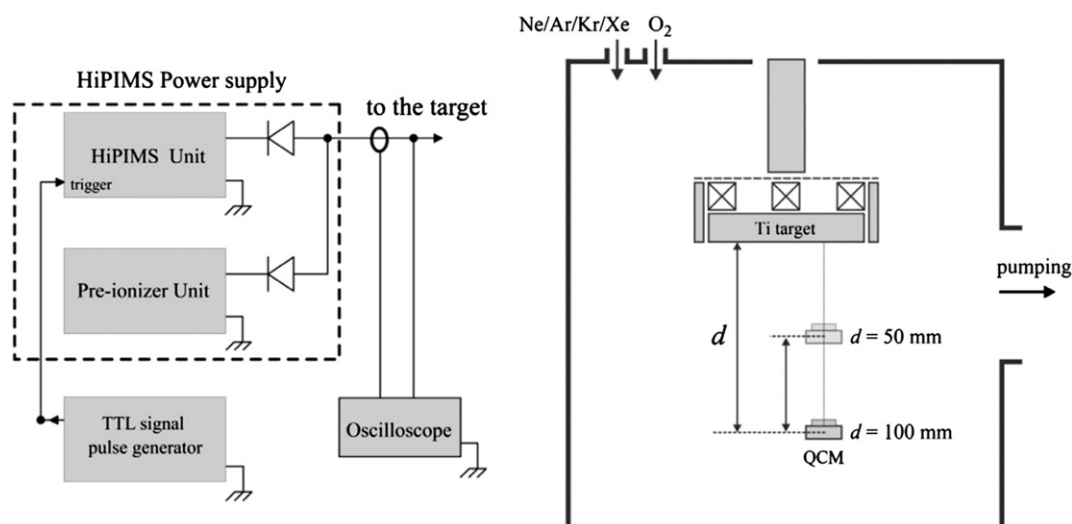

Fig. 1. Schematic representation of the experimental set-up. The QCM was moved axially with respect to the target into two positions; $d = 50$ to 100 mm.
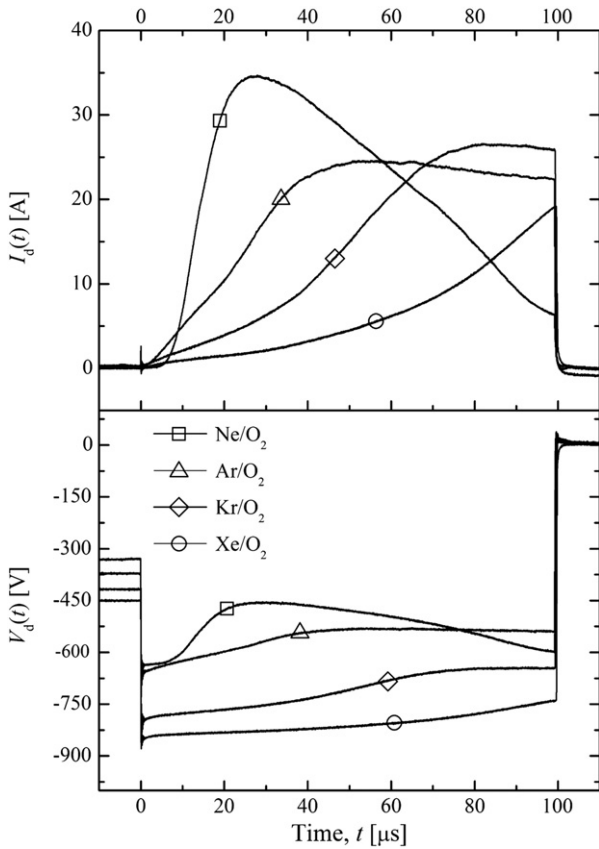
Fig. 2. The discharge current and potential waveforms for the HiPIMS discharges in the presence of the indicated gas mixtures. The average discharge power was maintained at a constant $P_{avg} = 100$ W for the cases of Ne/O$_2$, Ar/O$_2$ and Kr/O$_2$, however, $P_{avg} = 50$ W for the case of Xe/O$_2$.

power along with an associated decrease in average discharge current. The increase in the absolute target potential can be attributed to the lower secondary electron emission yield γ_{se} for heavier inert gases. For heavier inert gas ions, less energy is released during neutralization which results in a lower ion-induced potential secondary electron emission yield, γ_p. Since all discharges were operated in poisoned mode, changes in the secondary electron emission due to the target condition are ignored as the target is assumed, in all cases, to be completely covered by an oxide layer. Neglecting kinetic electron emission for values of $V_d < 1$ kV [4], then $\gamma_{se} \approx \gamma_p$ and the absolute potential applied to the target necessary to achieve a constant power would be larger for discharges containing heavier inert gases. The reduced average discharge current for heavier inert gas species is a consequence of maintaining a constant time-averaged discharge power using a larger target potential. The averaged discharge potential during the pulse on-phase was calculated as

$$V_{d\text{-avg}} = \frac{1}{\tau} \int_0^\tau V_d(t)\, dt; \tag{1}$$

and the average discharge current density was evaluated by

$$J_{d\text{-avg}} = \frac{1}{A_t \tau} \int_0^\tau I_d(t)\, dt. \tag{2}$$

where A_t is the area of the target. Fig. 3 shows the average target potential and average discharge current density during the pulse on-time calculated from the waveforms shown in Fig. 2 plotted against the mass
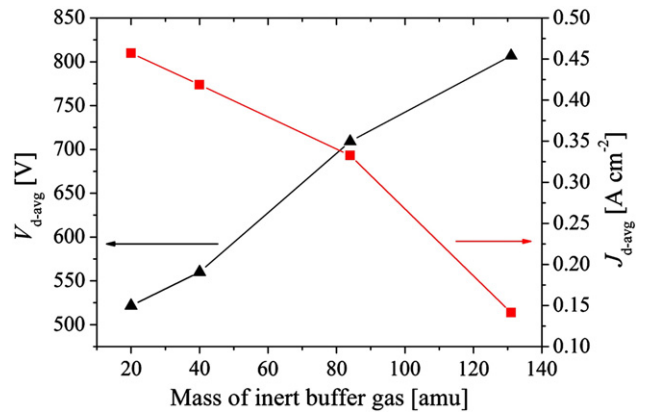

Fig. 3. The average pulse values of the target potential $V_{d\text{-avg}}$ (triangles) and of the target current density $J_{d\text{-avg}}$ (squares) versus the mass of the inert gas used in the mixture. These values correspond to the waveforms shown in Fig. 2.

of the inert gas mixed with oxygen. The average target voltage during the pulse on-time varies significantly between the gas mixtures, ranging from $V_{d\text{-avg}} = 521$ V for Ne/O$_2$ to $V_{d\text{-avg}} = 807$ V for Xe/O$_2$ with corresponding average current densities ranging from $J_{d\text{-avg}} = 0.46$ to 0.14 A/cm^2.

3.2. Deposition rates in reactive HiPIMS of titanium

The normalized deposition rates, D_n, measured using a QCM during reactive HiPIMS of titanium at two different axial distances from the target ($d = 50$ and 100 mm) for the four different gas mixtures are shown in Fig. 4. For an increased target-to-QCM distance, D_n was found to be lower for all gas mixtures. Sputter yields calculated using SRIM [23] are predicted to have a negative correlation with inert ion mass for a TiO$_2$ target (see Fig. 5), consequently one would expect a similar trend in the deposition rate. Furthermore, due to the decreasing average discharge current with increasing ion mass, it isn't unreasonable to expect a reduced value for D_n for discharges containing heavier inert gases. However, D_n was observed to increase with the mass of the inert gas (see Fig. 4), with the exception of the Xe/O$_2$ gas mixture at $d = 100$ mm. It is noted that during SRIM calculations, the default surface binding energy of titanium dioxide provided by SRIM was employed.
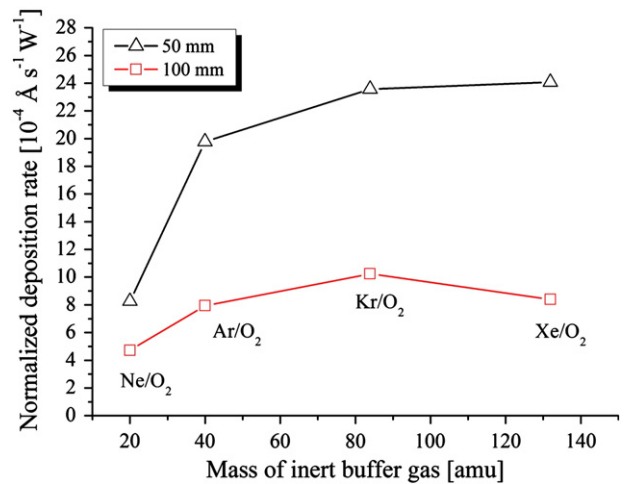

Fig. 4. Power normalized deposition rates measured at different axial distances d (50 and 100 mm) away from the target surface for the four gas mixtures during HiPIMS as a function of the inert gas mass.
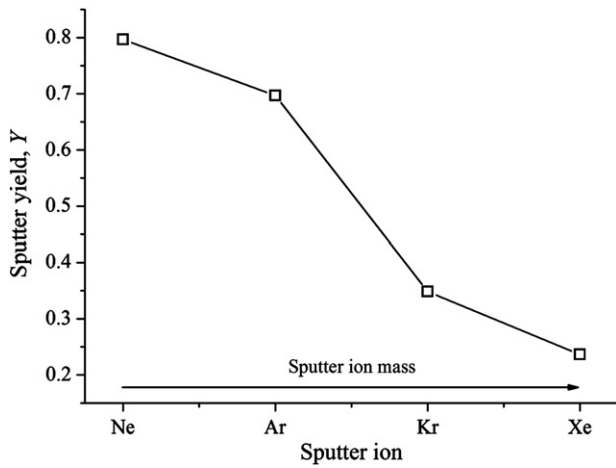
Fig. 5. SRIM predictions for the sputter yields, Y, of different inert gas ions normally incident upon a TiO$_2$ surface. Ion energies were assumed to be the value of $eV_{d\text{-avg}}$ measured for the different gas mixtures, where e is the elemental charge.

Fig. 6. Normalized values of $YV_{d\text{-avg}}^{-1/2}/(1 + \gamma_{se})$ calculated from the values shown in Fig. 3 and γ_{se} values obtained from using Eq. (4), used to illustrate the expected trend of the deposition rate as a function of inert gas mass. This, of course, excludes the affects of α and β (see Eq. (3)).

Based on the phenomenological model of HiPIMS developed by Vlcek and Burcalova [10], Capek et al. [5] obtained an expression for normalized deposition rate during HiPIMS operation:

$$D_n \propto (1 - \alpha\beta) \frac{V_{d\text{-avg}}^{-1/2}}{1 + \gamma_{se}}, \tag{3}$$

where α is the ionization fraction of sputtered particles ($0 \leq \alpha \leq 1$) and β is the probability of ionized sputtered vapour returning to the target surface ($0 \leq \beta \leq 1$). From Eq. (3), the yield effect dictates that any increase in the $V_{d\text{-avg}}$ results in a lower deposition rate normalized to the average discharge power by a factor that is approximated to be $V_{d\text{-avg}}^{-1/2}$, suggesting D_n should decrease with increasing inert gas mass according to the values of $V_{d\text{-avg}}$ shown in Fig. 3. However, a decrease in γ_{se} with increasing inert ion mass would suggest an increase in D_n. Although in HiPIMS, it is often the case that a significant fraction of the sputtering ions are back-attracted target ions and so the γ_{se} is a combination of the secondary electron emission due to sputtering by gas ions, γ_{mg}, and electron emission due to self sputtering, γ_{mm}, viz. $\gamma_{se} \sim \gamma_{mg}(1 - m_t) + \gamma_{mm} m_t$ where m_t is the fraction of target ions in the ion flux incident upon the target. However, the primary means of secondary electron emission is assumed to be ion-induced potential emission ($\gamma_{mg} \sim \gamma_p$), where the potential emission coefficient can be expressed as [24]:

$$\gamma_p \approx 0.032(0.78\varepsilon_{iz} - 2\phi), \tag{4}$$

where ε_{iz} is the ionization energy of the ion incident upon the target and ϕ is the work function for a metal target, or the energy gap for an insulating material. Due to the low ionization energy of titanium ($\varepsilon_{iz} = 6.83$ eV [25]) compared with twice its work function ($2\phi = 8.66$ eV [26]), the contribution to γ_{se} by self sputtering is low (i.e. $\gamma_{mg} \gg \gamma_{mm}$, hence $\gamma_{se} \sim \gamma_p$). For this simple treatment, multiply charged ions are neglected, the inert gas ions are considered to be the primary sputtering ions and the work function of titanium is assumed to be approximately equal to the energy required to liberate an electron from a titanium oxide surface (estimated by the energy gap of titanium oxide, 3.82 eV [27]).

Normalized values for $V_{d\text{-avg}}^{-1/2}/(1 + \gamma_p)$ were calculated by using the measured $V_{d\text{-avg}}$ shown in Fig. 3 and the γ_p values estimated from Eq. (4). The values of this factor were multiplied by the sputter yields, Y, predicted by SRIM and are displayed in Fig. 6. The relationship between the expected deposition rate and the sputter ion mass shown in Fig. 6 is very similar to sputter yields, Y, as predicted by SRIM calculations (see Fig. 5). For DCMS, $\alpha\beta \to 0$ and from Eq. (3), the decrease in D_n with increasing sputter ion mass is expected. However, $\alpha\beta > 0$ for HiPIMS and therefore the same trend may not hold. Furthermore, the
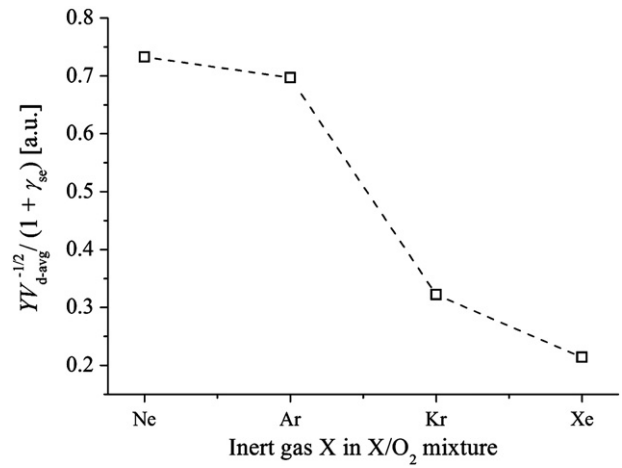
value of $\alpha\beta$ is expected to vary for different gas mixtures. Comparing the measured deposition rates in Fig. 4 and the trend of the factors affecting deposition rate shown in Fig. 6, $\alpha\beta$ must display a significant decrease for heavier inert gas mixtures. From [5]:

$$\beta \propto \frac{1}{V_{d\text{-avg}}}, \tag{5}$$

hence there is a reduced probability of ionized sputtered vapour returning to the target surface for heavier inert gases due to the increase in $V_{d\text{-avg}}$ (see Fig. 3), which is the reverse trend predicted by the yield effect. The ionization probability α is dependent on many parameters, the most obvious being the neutral flux from target surface, local electron temperature and the self-sputter yield. A systematic approach to analysing the effects of the inert gas choice for reactive HiPIMS on the parameters α and β warrants further investigation, but is beyond the scope of this contribution.

3.3. Comparison with reactive DCMS

The normalized deposition rates of TiO$_2$ for equivalent reactive DCMS discharges, using the same process conditions were also measured for a
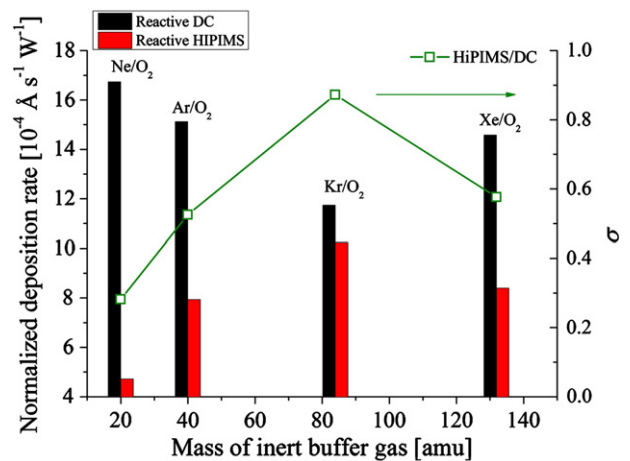

Fig. 7. Normalized deposition rate comparison between DCMS (black bar, left column) and HiPIMS (red bar, right column) for different inert gases mixed with oxygen, with the ratio, $\sigma = D_{HPM}/D_{DC}$, of the two values over plotted (open squares).

target-to-QCM distance $d = 100$ mm. Fig. 7 shows the comparison between the power normalized deposition rates for both HiPIMS (D_{HPM}) and DCMS (D_{DC}) of titanium in the presence of oxygen mixed with neon, argon, krypton or xenon alongside the ratio of the two: $\sigma = D_{HPM}/D_{DC}$.

In agreement with the predicted sputter yields given in Fig. 5, D_{DC} shows a decrease with inert gas mass, whereas D_{HPM} is observed to follow the inverse trend for the cases of neon, argon and krypton. Consequently, σ increases markedly for increasing inert gas mass mixed with oxygen, with the exception of the Xe/O$_2$ gas mixture. Due to the lower average discharge power used for the Xe/O$_2$ mixture (50 W compared with 100 W) and the significantly lower peak current density recorded during the pulse on-time, the racetrack width is expected to be lower [28], thereby reducing the active area of the target which could lead to a reduction in deposition rate relative to the other gas mixtures. Furthermore, in the formulation of Eq. (3), the potential drop within the discharge is assumed to occur only within the cathode sheath such that the ions impinging upon the target are taken to possess energies equal to the applied target potential. However, as the plasma possesses finite impedance, a portion of the potential drop necessarily occurs across the plasma itself and not exclusively within the cathode sheath. As a result, the energy of the impinging ions is likely to be somewhat lower than assumed, consequently reducing the predicted sputter yield and by extension, the expected deposition rate [29]. It is conjectured that a higher proportion of the applied target potential is dropped over the Xe/O$_2$ plasma bulk when compared with the other gas mixtures, given the comparatively larger mass of xenon. If this is the case, a proportional reduction in the incident ion energy follows and hence a discrepancy between the measured and expected deposition rate will arise.

For the case of Kr/O$_2$, not only is the normalized deposition rate observed to be higher than for Ar/O$_2$ in HiPIMS operation, it is also comparable to the value measured in reactive DCMS: $\sigma = 0.87$. Additionally, high-energy negative ion production at the target surface is expected to be reduced in a Kr/O$_2$ discharge when compared with the case of Ar/O$_2$. This is because, in general, the intensity of high-energy O$^-$ ions impinging upon the substrate decreases with the secondary electron emission coefficient [30].

Taking into consideration that no optimization of the process conditions was attempted in this investigation, it seems plausible that employing krypton as the buffer gas alongside oxygen during reactive HiPIMS of titanium in favour of argon would be beneficial in terms of the power normalized deposition rate as well as reducing detrimental effects caused by energetic negative ion bombardment. The effect of high-energy negative ion bombardment on the deposited film during HiPIMS in the presence of different inert gases is the subject of an upcoming contribution.

4. Conclusions

The deposition rates in reactive HiPIMS of titanium in the presence of oxygen and one of four different inert gases (Ne, Ar, Kr and Xe) have been measured by means of a quartz crystal microbalance located directly above the target erosion track. The power normalized deposition rates, D_n, were found to increase with the mass of inert gas with the exception of the Xe/O$_2$ gas mixture. This is contrary to the trend expected by both the yield effect and predictions based on sputter yield calculations by SRIM. The Kr/O$_2$ gas mixture produced the highest measured value for $D_n = 1.02 \times 10^{-3}$ Å s^{-1} W^{-1}. The observed increase of D_n with the mass of inert gas was partially attributed to a decreased return effect in the heavier gases. However, it was concluded

that additional work must be done in order to ascertain the determining mechanism governing this correlation. Additionally, it was found that DCMS and HiPIMS displayed opposing trends of normalized deposition rate with the mass of inert gas used, again with the exception of the Xe/O$_2$ case. The deviations from the trends in deposition rates for both DCMS and HiPIMS in the case of Xe/O$_2$ are thought to arise from differences in the plasma impedance and the erosion racetrack width, which affect the energy of sputter ions and the active target area, respectively. Interestingly and despite no optimization, the ratio of the two deposition rates was close to unity for the case of Kr/O$_2$; the normalized deposition rate of HiPIMS was found to be 87% of the value recorded in DCMS. However, it remains to be determined whether krypton offers additional advantages compared with other inert gases beyond an apparent increase in normalized deposition rate and a predicted decrease in the amount of high energy negative ions ejected from the target surface.

References

[1] V. Kouznetsov, U.S. patent 6296742 B1 (issued 2001).
[2] U. Helmersson, M. Lattemann, J. Alami, J. Bohlmark, A.P. Ehiasarian, J.T. Gudmundsson, Society of Vacuum Coaters 48th Annual Technical Conf. Proc. (Denver, CO, 23–28 April 2005), 2005, p. 458.
[3] M. Samuelsson, D. Lundin, J. Jensen, M.A. Raadu, J.T. Gudmundsson, U. Helmersson, Surf. Coat. Technol. 205 (2010) 591.
[4] A. Anders, J. Vac. Sci. Technol. A 28 (2010) 783.
[5] J. Capek, M. Hala, O. Zabedia, J.E. Klemberg-Sapieha, L. Martinu, J. Phys. D. Appl. Phys. 46 (2013) 205205.
[6] D.J. Christie, J. Vac. Sci. Technol. A 23 (2005) 330.
[7] J. Emmerlich, S. Mráz, R. Snyders, K. Jiang, J.M. Schneider, Vacuum 82 (2008) 867.
[8] D. Lundin, P. Larsson, E. Wallin, M. Lattemann, N. Brenning, U. Helmersson, Plasma Sources Sci. Technol. 17 (2008) 035021.
[9] P. Poolcharuansin, B. Liebig, J.W. Bradley, Plasma Sources Sci. Technol. 21 (2012) 015001.
[10] J. Vlcek, K. Burcalova, Plasma Sources Sci. Technol. 19 (2010) 065010.
[11] M. Scherer, P. Wirz, Thin Solid Films 119 (1984) 203.
[12] M. Zeuner, H. Neumann, J. Zalma, H. Biederman, J. Appl. Phys. 83 (1998) 5083.
[13] S. Mráz, J.M. Schneider, Appl. Phys. Lett. 89 (2006) 051502.
[14] S. Mahieu, W.P. Leroy, K. Van Aeken, D. Depla, J. Appl. Phys. 106 (2009) 093302.
[15] P. Pokorný, M. Mišina, J. Bulíř, J. Lančok, P. Fitl, J. Musil, M. Novotný, Plasma Process. Polym. 8 (2011) 459–464.
[16] T. Welzel, S. Naumov, K. Ellmer, J. Appl. Phys. 109 (2011) 073302.
[17] M. Bowes, P. Poolcharuansin, J.W. Bradley, J. Phys. D. Appl. Phys. 46 (2013) 045204.
[18] K. Sarakinos, J. Alami, M. Wuttig, J. Phys. D. Appl. Phys. 40 (2007) 2108.
[19] R. Chistyakov, U.S. patent 6896773 (issued 2005).
[20] K. Sarakinos, J. Alami, C. Klever, M. Wuttig, Surf. Coat. Technol. 202 (2008) 5033.
[21] V. Stranak, A.-P. Herrendorf, H. Wulff, S. Drache, M. Cada, Z. Hubicka, M. Tichy, R. Hippler, Surf. Coat. Technol. 222 (2013) 112.
[22] P. Poolcharuansin, B. Liebig, J.W. Bradley, IEEE Trans. Plasma Sci. 38 (2010) 3007.
[23] , (available at) www.srim.org.
[24] R.A. Baragiola, E.V. Alonso, J. Ferron, A. Oliva-Florio, Surf. Sci. 90 (1979) 240.
[25] A.M. James, M.P. Lord, MacMillan's Chemical and Physical Data, Macmillan Press, London, 1992.
[26] D.R. Lide (Ed.), CRC Handbook of Chemistry and Physics, Eighty fourth ed., CRC Press, Boca Raton, Florida, 2003, pp. 12–130.
[27] N. Sakai, Y. Ebina, K. Takada, T. Sasaki, J. Am. Chem. Soc. 126 (2004) 5851.
[28] G. Clarke, A. Mishra, P.J. Kelly, J.W. Bradley, Plasma Process. Polym. 6 (2009) S548.
[29] A. Anders, Society of Vacuum Coaters 51st Annual Technical Conf. Proc. (Chicago, IL, 19–24 April 2008), 2008, p. 271.
[30] S. Mahieu, D. Depla, Appl. Phys. Lett. 90 (2007) 121117.